Case Studies in Thermal Engineering 22 (2020) 100798

Contents lists available at ScienceDirect

Case Studies in Thermal Engineering

journal homepage: http://www.elsevier.com/locate/csite

Importance of multiple slips on bioconvection flow of cross nanofluid past a wedge with gyrotactic motile microorganisms

Ali Saleh Alshomrani [a,*], Malik Zaka Ullah [a], Dumitru Baleanu [b,c]

[a] Department of Mathematics, Faculty of Science, King Abdulaziz University, Jeddah, Saudi Arabia
[b] Department of Mathematics, Cankaya University, Turkey
[c] Institute of Space Sciences, Magurele-Bucharest, Romania

ARTICLE INFO

Keywords:
Magneto cross nanofluid
Multiple slip effects
Wedge shape geometry
Motile microorganisms
Bio-convection
Activation energy

ABSTRACT

In the current article, a mathematical model is developed to visualize the flow of non-Newtonian magneto cross nanofluid with mass and heat transport rates having activation energy, motile microorganisms and bioconvection over the wedge. The phenomena of microorganisms is implemented to control the suspension of nanomaterials. The results of hydromagnetic are also integrated into the momentum expression. Nanofluid is developed by dispersing the nanosized particles in the regular fluid. Nanosized solid materials like carbides, ceramics, graphene, metal, alloyed CNTs etc. have been utilized for the preparation of nanofluid. Physically regular fluids have low thermal efficiency. Therefore, the nanosize particles can be utilized to enhance the thermal efficiency of the regular fluids. Nanofluids have many features in hybrid power engine, heat transfer and can be useful in cancer therapy and medicine. The constructed system is first simplified into nonlinear form by introducing similarity variables. Then obtained ordinary differential equations (ODEs) which are evaluated for numerical solution. Further, for numerical approximation, the popular bvp4c scheme built-in function in MATLAB is utilized. Reliable outcomes are achieved for the temperature, velocity, concentration and motile microorganism density profiles. Results for numerous essential flow parameters are shown via numerical outcomes and graphs. It is revealed that velocity upsurges with enhancement in mixed convection parameter while reduces for bioconvection Rayleigh and buoyancy ratio parameters. Furthermore, the volumetric concentration of nanoparticles boost up for growing estimations of activation energy parameter. The microorganisms field upsurges with larger microorganism slip parameters while reduces with the augmentation in magnitude of bioconvection Lewis number and Peclet number. The obtained numerical results are compared with the available data and found good agreement.

1. Introduction

Nanofluids are the suspension of nanomaterials in liquid that produce a significant change in their characteristics at modest concentration of nanomaterials. Currently, many researchers are working on nanofluids to modify their behavior so that it can be useful in different fields of life, where thermal efficiency improvement is prominent. Moreover, nanofluids are commonly used in nuclear power plants, transportation, telecommunications, electronics, bioengineering, agricultural engineering and nutrition. The

* Corresponding author.
E-mail address: aszalshomrani@kau.edu.sa (A.S. Alshomrani).

https://doi.org/10.1016/j.csite.2020.100798
Received 6 October 2020; Received in revised form 25 November 2020; Accepted 28 November 2020
Available online 2 December 2020

Nomenclature

u, v	Components of velocity $[m.s^{-1}]$
x, y	Space coordinates $[m]$
Ha	Hartmann number
B_0	Magnetic field strength $[N.m^{-1}.A^{-1}]$
U_0	Reference velocity $[m.s^{-1}]$
$u_w(x)$	Stretching velocity $[m.s^{-1}]$
$u_e(x)$	Free stream velocity $[m.s^{-1}]$
$(\rho c)_p$	Nanoparticle specific heat $[J.kg^{-3}.K^{-1}]$
$(\rho c)_f$	Heat capacity of fluid $[J.kg^{-3}.K^{-1}]$
u_{slip}	Velocity slip $[m.s^{-1}]$
T_{slip}	Thermal slip $[K]$
C_{slip}	Concentration slip
N_{slip}	Microorganism slip
$Q(x)$	heat generation/absorption coefficient
Pr	Prandtl number
L, P, Q_1, R	Velocity slip factor [s/m], temperature, concentration and microorganism slip factors $[m]$
Rc	Bio-convection Rayleigh parameter
Rb	Buoyancy ratio number
Nb	Brownian motion parameter
S	Mixed convection parameter
Nt	Thermophoresis parameter
E_a	Activation energy
Le	Lewis number
We	Weissenberg number
Pe	Peclet number
Lb	Bioconvection Lewis number
B_1	Thermal slip parameter
B_2	Solutal slip parameter
B_3	Microorganism slip parameter
Re_x	Reynolds number
Nu_x	Local Nusselt number
Sh_x	Local Sherwood number
Sh_n	Local microorganism density number
N_∞	Ambient fluid microorganisms
T_∞	Ambient fluid temperature $[K]$
C_∞	Ambient fluid concentration
D_B	Brownian diffusion coefficient $[m^2.s^{-1}]$
D_m	Microorganisms diffusion coefficient $[m^2.s^{-1}]$
D_T	Thermophoresis diffusion coefficient $[m^2.s^{-1}]$
k_∞, D_∞	Ambient thermal conductivity
b	Chemotaxis constant $[m]$
m	Fitted rate constant
W_c	Cell swimming speed $[m.s^{-1}]$
C_w	Concentration at the surface
N_w	Microorganisms at the surface
T_w	Temperature at the surface $[K]$
f	Dimensionless velocity
N	Microorganism field
Kr	Chemical reaction constant

Greek symbols

ω_1	Thermal conductivity parameter
ω_2	Concentration conductivity parameter
ω_3	Microorganism conductivity parameter
α_1	Velocity slip parameter
σ	Electrical conductivity $[S.m^{-1}]$

σ^*	Chemical reaction parameter
α^*	Thermal diffusivity $[m^2.s^{-1}]$; ω Temperature difference parameter
δ_1	Microorganism concentration difference parameter
δ_0	Heat generation parameter
τ	Heat capacity ratio
q_w	Thermal mass flux
q_m	Solutal mass flux
q_n	Microorganism mass flux
φ	Volumetric concentration
θ	Temperature distribution
χ	Microorganism concentration
g	Gravity $[m.s^{-2}]$
ρ_f	Fluid density $[kg.m^{-3}]$
ρ_m	Microorganisms density $[kg.m^{-3}]$
ρ_p	Nanoparticles density $[kg.m^{-3}]$
ν	Kinematic viscosity $[m^2.s^{-1}]$
$\psi(x,y)$	Stream function
ζ	Dimensionless variable
γ	Wedge angle parameter
Ω	Angle of the wedge
Λ	Cross time constant

current article is proposed to examine the behavior of nanofluids in different fields and also discuss the enhanced heat transfer characteristics of nanofluids. Initially, it was investigated in the Argonne National Laboratory (ANL) of the USA in 1905 by Choi and Eastman [1]. Such fluids offer the possibility of stirring because of their enhanced convection as compare to regular fluids. The main objective of nanofluids is the higher thermal conductivity potential according to base fluids and higher stability according to micro-particles or nano-particles. Buongiorno [2] has discussed the Brownian motion and thermophoresis features of nanofluid. Raju et al. [3] studied improvement of convection by using nanoliquid in the case of heat absorption/generation. Sheikholeslami and Ganji [4] analyzed the method of heat transfer by utilizing nanofluid. Sheikholeslami and Bhatti [5] described the influences of fluid objects forms in the background of a strong gravitational field. Hsiao [6] examined the magnetohydrodynamic Carreau nanoliquid flow and suggested that investigated findings are beneficial for improvement of different thermal conductivity processes. Turkyilmazoglu [7] inspected the nanoliquid flow via Buongiorno's relation in asymmetric tube. Khan and Shehzad [8] investigated Brownian motion and thermophoresis characteristics of nanomaterials flow over a moving configuration. Waqas et al. [9] used multiple slip characteristics in the flow of nanomaterials across a rotating disk in the appearance of microorganisms. Hassan et al. [10] assessed the characteristics of the transfer of heat over the wave layer through the nanofluid flow. Many researchers admit the significance of nanofluid and have suggested ultimate results [11–25].

Raju et al. [26] studied aspects of the cross-diffusion consequences on the MHD flow of Carreau fluid across a moving sheet with non-uniform temperature source/sink. Sultan et al. [27] explored the numerical treatment of mixed convective Carreau fluid flow with multiple wedge slips. Mahanthesh et al. [28] studied the efficacy of Hall's current and incremental source of heat in the non-linear heat transfer rate of dusty TiO2-EO nanofluids with nonlinear radiative effects. Mahanthesh et al. [29] also investigated the effects of MHD flow of SWCNT and MWCNT nanofluids on such a rotating stretching disk with the thermal and exponential space-dependent heat source.

The activation energy initially proposed by Svante Arrhenius in 1889. Activation energy is the basic energy given by the reagents for conversion into materials for different chemical responses. Potential and kinetic energies related with molecules are useful to snapping of bonds or to the stretching and twisting of bonds. Maleque [30] examined the consequences of endothermic/exothermic chemical processes on flat disk subject to activation energy and permeable medium. Awad et al. [31] conducted another relative analysis to discuss activation energy impact utilizing Newtonian model. More work on activation energy can be seen via attempts [32, 33].

The macroscopic flow of convective liquid particles resulting from a transition in the presence of a density gradient is termed as bio-convection. Macroscopic motion is caused by floating microorganisms which changed the composition of the nanofluid. Bioconvection has a wide range of applications in the natural sciences, biotechnology, microsystems, bioinformatics fields, nanomaterials and micro-fluidic techniques. Bioconvection also plays a major role in engineering in which the electromagnetic field is utilized to set up a bioconvection process for the manufacturing of mechanical energy and power resources. A further important characteristic of bio-convection is the aggregation of nanotechnology with motile microorganisms that enhances the stability, heat and mass transport of nanomaterials. In addition, to obtain substantial bio-convection, microbial thermal transfer is managed by a variety of carbon, light, biochemical inputs, inertia and gravitational rotational velocity that are often difficult to achieve in nanofluids. Virtually, this microbial movement in liquids can be associated with the purification of microorganism's cells and differentiation of various strains. Kuznetsov [34] addressed the bioconvection of nanomaterials across the convectively heated plate subject to gyrotactic micro-organisms. Kuznetsov and Avramenko [35] discussed the idea of bioconvection with the suspension of gyrotactic

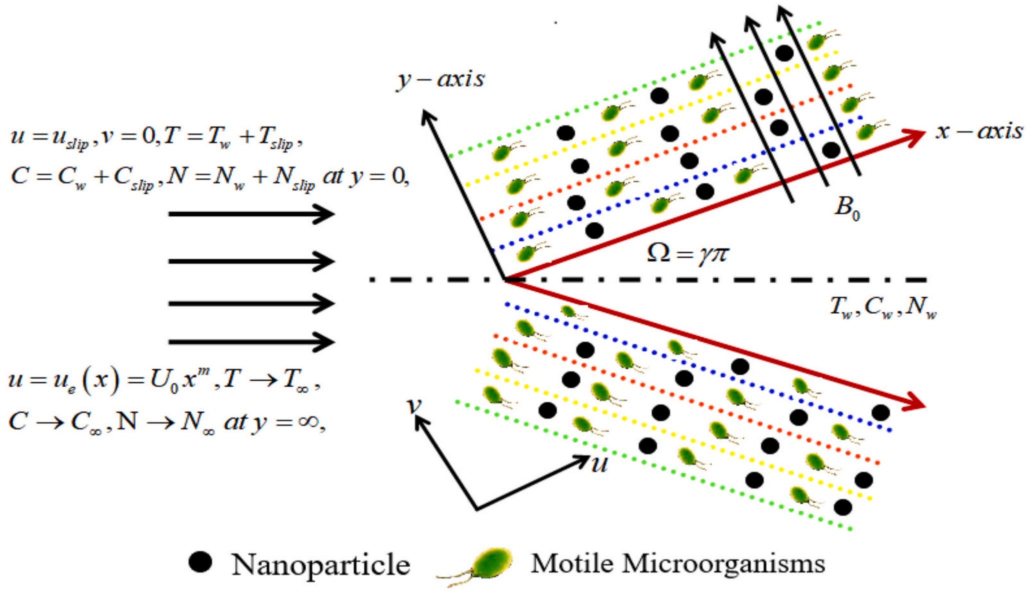

Fig. 1. A schematic of the wedge in a magneto-cross nanofluid.

microorganisms. Khan et al. [36] observed influences of gyrotactic micro-organisms in magneto Burgers nanoliquid flow. Bio-convective nanofluids flow subject to different thermo-physical characteristics is achieved by Begum et al. [37]. Waqas et al. [38] examined heterogeneous movement of nanoparticles in presence of gyrotactic micro-organisms. Zohra et al. [39] investigated bio-convection slip flow of viscous liquid through a spinning rotating cone. Uddin et al. [40] developed a well-known numerical approach namely the Chebyshev collocation procedure for the analysis of the rheological existence of the Newtonian fluid in the presence of sliding microorganisms. Naz et al. [41] analyzed the dynamics of magnetohydrodynamic (MHD) cross nanofluid with gyrotactic motile microorganisms, bio-convection and entropy generation. Mohamed et al. [42] examined the experimental analysis of micro-bioconvective flow utilizing the Adomian process of decomposition. Ansari et al. [43] analyzed the magnetohydrodynamic bioconvective Casson nanofluid flow via finite element analysis through paired quasilinearisation. Hassan et al. [44] investigated the bioconvection flow of modified second-grade nanofluids subject to nanotubes and gyrotactic motile microorganisms. Wang et al. [45] scrutinized effective Prandtl impacts on bio-convective thermally proposed magnetized tangent hyperbolic nanofluids with micro-organisms and second-order velocity slip. Khan et al. [46] analyzed the bioconvection of couple-stress nanoliquids subject to activation energy and Wu's slip. More work on this topic is seen via studies [47–49].

The main survey in this article examines the impacts of numerous slips in the cross-magneto-nanofluid bioconvection flow past the wedge. Embedded ordinary differential equations are resolved mathematically by using built-in solver bvp4c. Furthermore, Lobatto-IIIa formula is implemented with tolerance 10^{-6}. The outcomes of interesting variables against the flow field are discussed and elaborated through graphical and tabular data. The presented work plays a major role in engineering in which the electromagnetic field is utilized to set up a bioconvection process for the manufacturing of mechanical energy and power resources. A further important characteristic of bioconvection is the aggregation of nanotechnology with motile microorganisms that enhances the stability, heat and mass transport of nanomaterials. In addition, to obtain substantial bio-convection, microbial thermal transfer is managed by a variety of carbon, light, biochemical inputs, inertia and gravitational rotational velocity that are often difficult to achieve in nanofluids.

2. Mathematical formulation of the flow

Two-dimensional MHD cross nanofluid flow across a wedge geometry has been formulated. The significance of bioconvection, multiple slips, activation energy, velocity, thermal distribution, the concentration of nanoparticles and the rescaled density of motile microorganisms are also scrutinized in the presence of nano-shaped particles. Here coordinates system is chosen as the x-axis is along with the flow geometry and magnetic strength is parallel to the y-axis direction. Geometry of the flow model is captured through Fig. 1.

The governing equations related to the above assumptions are given bellow [17,27,50,51]:

2.1. Equation of continuity

$$\frac{\partial u}{\partial x}+\frac{\partial v}{\partial y}=0 \qquad (1)$$

2.2. Equation of momentum

$$u\frac{\partial u}{\partial x}+v\frac{\partial u}{\partial y}=u_e\frac{du_e}{dx}+\nu\frac{\partial}{\partial y}\left[\frac{\frac{\partial u}{\partial y}}{1+\left(\Lambda\frac{\partial u}{\partial y}\right)^n}\right]-\frac{\sigma B_0^2}{(\rho c)_f}(u-u_e)$$
$$+\frac{1}{\rho_f}\left[(1-C_f)\rho_f\beta^* g(T-T_\infty)-(\rho_p-\rho_f)g(C-C_\infty)-(N-N_\infty)g\gamma^{**}(\rho_m-\rho_f)\right], \tag{2}$$

where u_e depicts free stream velocity, ρ_f density of fluid, n power-law index, Λ cross-time constant, $(\rho c)_f$ heat capacity of fluid, B_0 magnetic strength, σ electric conductivity, g gravitational acceleration, ρ_p density of the fluid, ρ_m density of motile microorganisms and ν kinematic viscosity.

2.3. Equation of energy

$$u\frac{\partial T}{\partial x}+v\frac{\partial T}{\partial y}=\frac{1}{(\rho c)_f}\frac{\partial}{\partial y}\left[k(T)\frac{\partial T}{\partial y}\right]+\tau\left\{D_B\frac{\partial C}{\partial y}\frac{\partial T}{\partial y}+\frac{D_T}{T_\infty}\left(\frac{\partial T}{\partial y}\right)^2\right\}+\frac{Q}{\rho c_p}(T-T_\infty), \tag{3}$$

where $k(T)$ is mass diffusivity for cross fluid which can be defined as [66]:

$$k(T)=k_\infty\left[1+\in_1\frac{T-T_\infty}{T_w-T_\infty}\right], \tag{4}$$

2.4. Equation of concentration

$$u\frac{\partial C}{\partial x}+v\frac{\partial C}{\partial y}=\frac{\partial}{\partial y}\left[D(C)\frac{\partial C}{\partial y}\right]+\frac{D_T}{T_\infty}\frac{\partial^2 T}{\partial y^2}-Kr^2(C-C_\infty)\left(\frac{T}{T_\infty}\right)^m\exp\left(\frac{-E_a}{\kappa T}\right), \tag{5}$$

where Kr depicts constant chemical reaction, $D(C)$ mass diffusivity, m fitted rate constant, and E_a activation energy. The mass diffusivity is addressed as [66]:

$$D(C)=D_\infty\left[1+\in_2\frac{C-C_\infty}{C_w-C_\infty}\right], \tag{6}$$

2.5. Equation of motile microorganisms

$$u\frac{\partial N}{\partial x}+v\frac{\partial N}{\partial y}=D_m\left(\frac{\partial^2 N}{\partial y^2}\right)-\frac{bW_c}{(C_w-C_\infty)}\left[N\frac{\partial^2 C}{\partial y^2}+\frac{\partial C}{\partial y}\frac{\partial N}{\partial y}\right], \tag{7}$$

where D_m shows coefficient of microorganism's diffusion, b chemotaxis constant and W_c cell swimming speed.

2.6. Boundary conditions

The boundary restrictions are

$$u=u_{slip},\ v=0,\ T=T_w+T_{slip},\ C=C_w+C_{slip}, N=\ N_w+N_{slip}\ at\ y=0, \tag{8}$$

$$u=u_e(x)=U_0x^m,\ T\to T_\infty,\ C\to C_\infty, N\to N_\infty\ at\ y=\infty, \tag{9}$$

where T_w depicts temperature at the wall, C_w concentration of nanoparticle at surface and N_w density of motile microorganisms at the surface and $u_{slip}, T_{slip}, C_{slip} N_{slip}$ wall velocity, thermal, concentration of nanoparticles and rescaled density of motile microorganisms slips respectively. Mathematically [52]:

$$u_{slip}=L\frac{\partial u}{\partial y}\left[\left(1+\left(\Lambda\frac{\partial u}{\partial y}\right)^n\right)^{-1}\right], \tag{10}$$

$$T_{slip}=P\frac{\partial T}{\partial y}, C_{slip}=Q_1\frac{\partial C}{\partial y}, N_{slip}=R\frac{\partial N}{\partial y}, \tag{11}$$

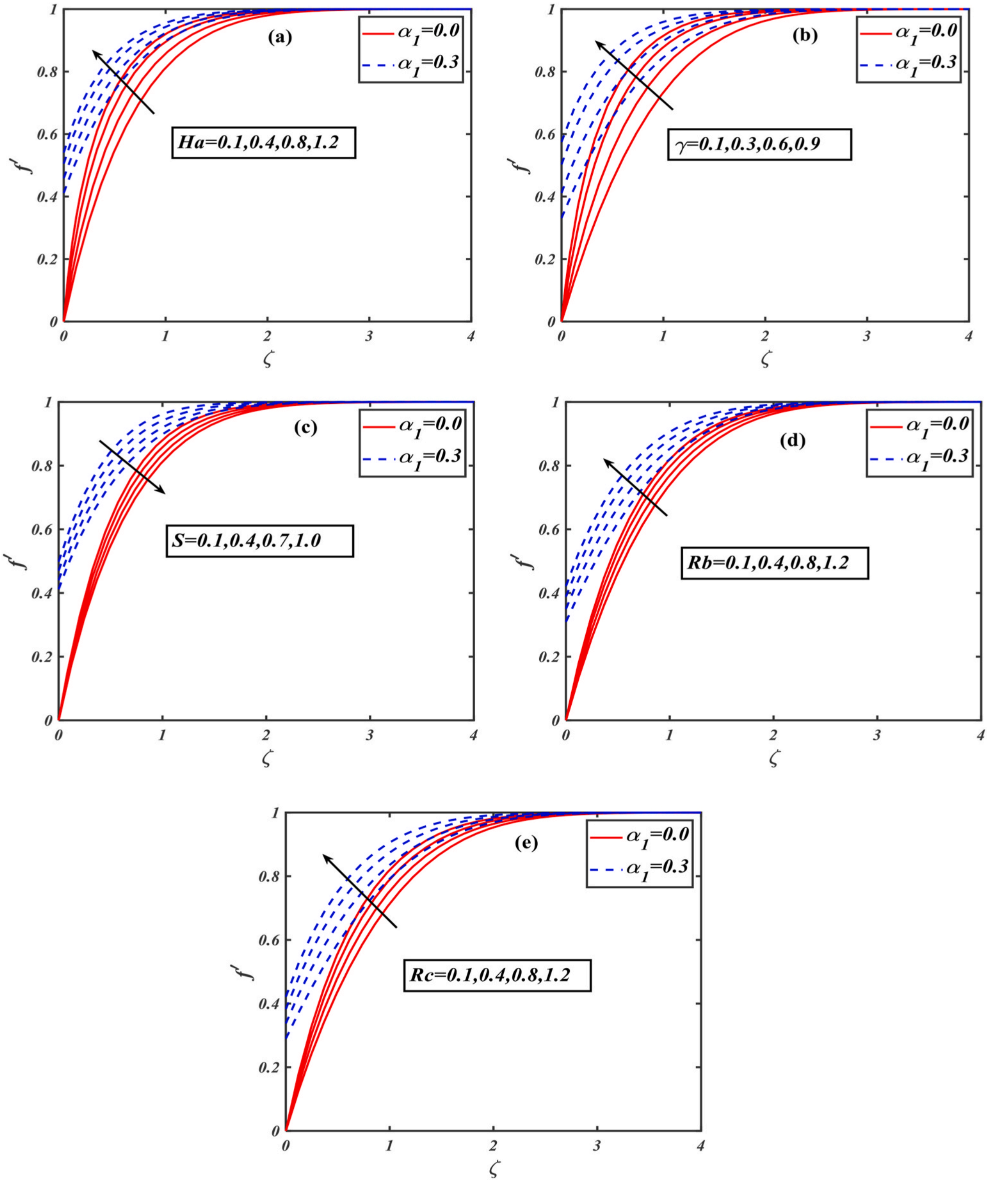

Fig. 2. Significane of *Ha*, *γ*, *S*, *Rb*, *Rc* on f'.

where L,P,Q and $R$are Navier, thermal, volumetric concentration and rescaled density of motile microorganisms slip coefficients correspondingly.

2.7. Similarity analysis

The dimensionless variables are taken as [51,61]:

$$\left.\begin{aligned}&\psi(x,y)=\sqrt{\frac{2\nu xU_e}{m+1}}x^{\frac{m+1}{2}}f(\zeta),\ \zeta=y\sqrt{\frac{(m+1)U_e}{2\nu}}x^{\frac{m-1}{2}}\\&\theta(\zeta)=\frac{T-T_\infty}{T_w-T_\infty},\ \varphi(\zeta)=\ \frac{C-C_\infty}{C_w-C_\infty},\chi(\zeta)=\ \frac{N-N_\infty}{N_w-N_\infty}\end{aligned}\right\},\tag{12}$$

where ψ shows stream function, $f(\zeta)$ dimensionless velocity, $\theta(\zeta)$ dimensionless temperature and $\varphi(\zeta),\chi(\zeta)$ volumetric concentration of nanoparticles and rescaled density of microorganisms respectively, T temperature of the fluid, C fluid concentration and N mortality of fluid. Equation (1) is satisfied while Eqs. (2)–(9) take the following forms:

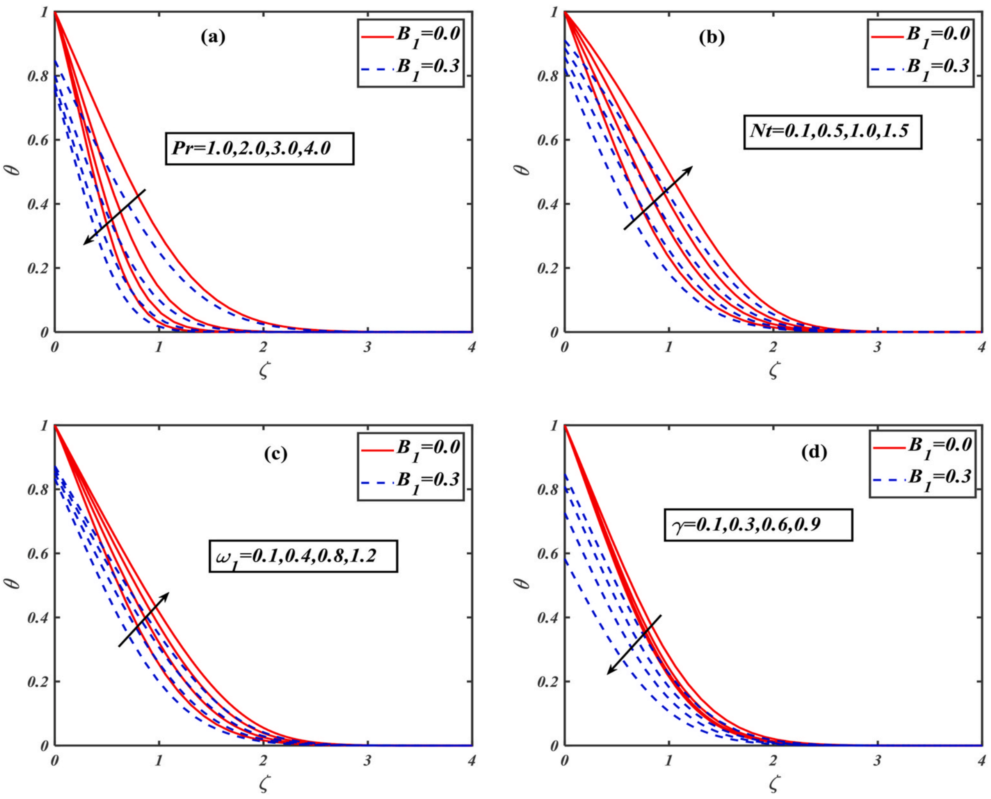

Fig. 3. Significane of Pr, Nt, ω_1, γ on θ.

$$[1+(1-n)(Wef'')^n]f''' + [ff'' + Ha^2(1-f')][1+(Wef'')^n]^2 \\ +\gamma\left[1-(f')^2\right][1+(Wef'')^n]^2 + S(\theta - Rb\varphi - Rc\chi) = 0, \tag{13}$$

$$(1+\omega_1\theta)\theta'' + \omega_1(\theta')^2 + Prf\theta' + Pr\left(Nb\theta'\varphi' + Nt\theta'2\right) + \delta_0 Pr\theta = 0, \tag{14}$$

$$(1+\omega_2\varphi)\varphi'' + \omega_2(\varphi')^2 + \left(\frac{Nt}{Nb}\right)\theta'' + Le\Pr[f\varphi'] - \Pr Le\sigma(1+\omega\theta)^m \exp\left(\frac{-E_a}{1+\omega\theta}\right)\varphi = 0, \tag{15}$$

$$(1+\omega_3\chi)\chi'' + \omega_3\chi'^2 + Lbf\chi' - Pe(\varphi''(\chi+\delta_1) + \chi'\varphi') = 0, \tag{16}$$

$$\left.\begin{array}{l} f(0)=0,\ f'(0)=\dfrac{\alpha_1}{\sqrt{2-\gamma}}f''(0)\left[\dfrac{1}{1+(Wef'(0))^n}\right], \\ f'(\infty)\to 1, \\ \theta(0)=1+\dfrac{B_1}{\sqrt{2-\gamma}}\theta'(0),\ \theta(\infty)\to 0, \\ \varphi(0)=1+\dfrac{B_2}{\sqrt{2-\gamma}}\varphi'(0),\ \varphi(\infty)\to 0, \\ \chi(0)=1+\dfrac{B_3}{\sqrt{2-\gamma}}\chi'(0),\ \chi(\infty)\to 0, \end{array}\right\}, \tag{17}$$

The variables appearing in Eqs. (13)-(17) are local Weissenberg number We, Prandtl number Pr, Lewis number Le, Hartmann number Ha, temperature difference parameter ω, mixed convection parameter S, buoyancy ratio parameter Rb, bioconvection Rayleigh number Rc, Brownian motion parameter Nb, thermophoresis parameter Nt, wedge angle parameter γ, heat source-sink parameter δ_0, motile microorganisms difference parameter δ_1, Peclet number Pe, bioconvection Lewis number Lb, velocity slip parameter α_1, thermal slip parameter B_1, solutal slip parameter B_2 and density of motile microorganisms slip parameter B_3 which are expressed by

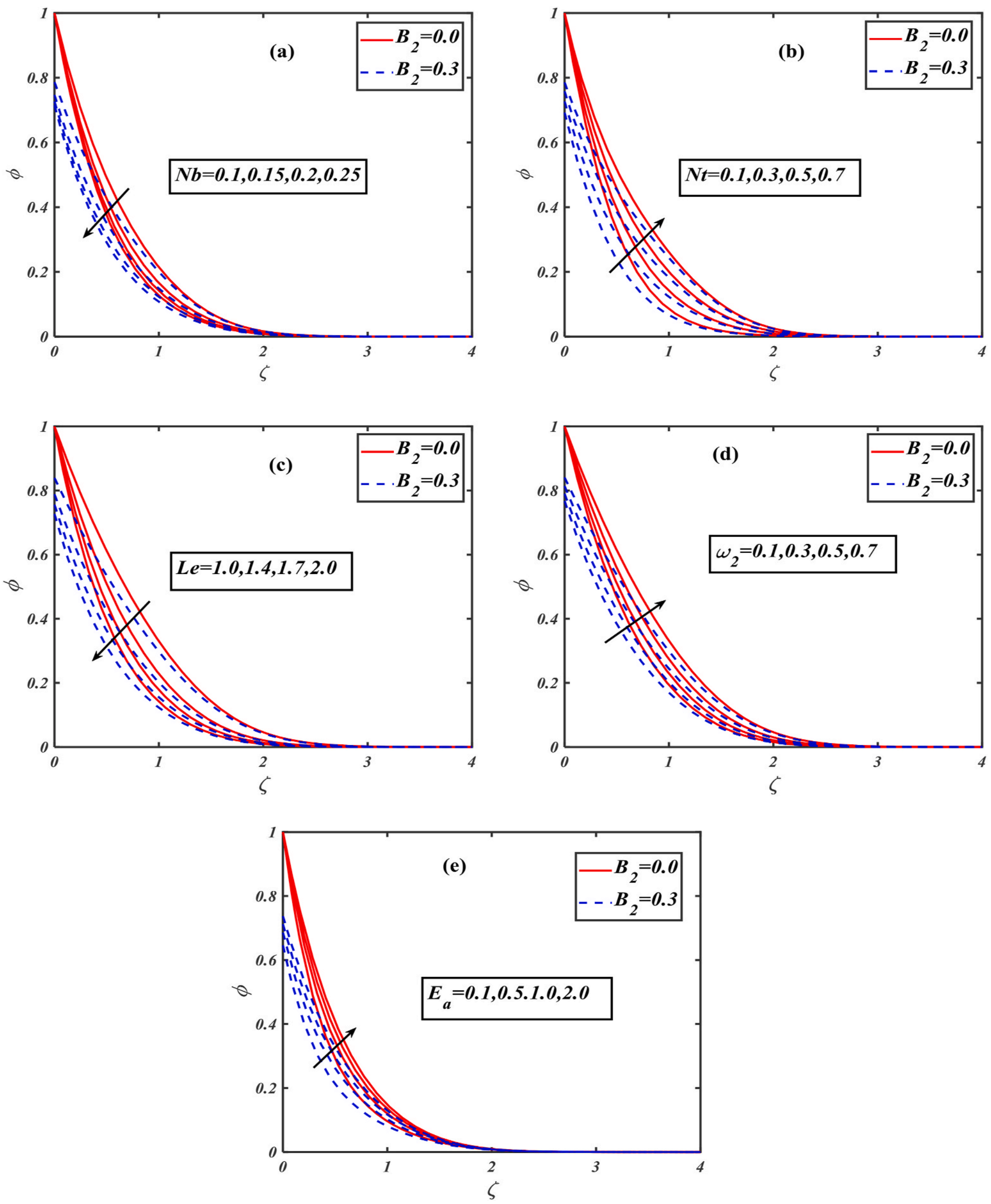

Fig. 4. Significane of Nb, Nt, Le, ω_2, E_a on φ.

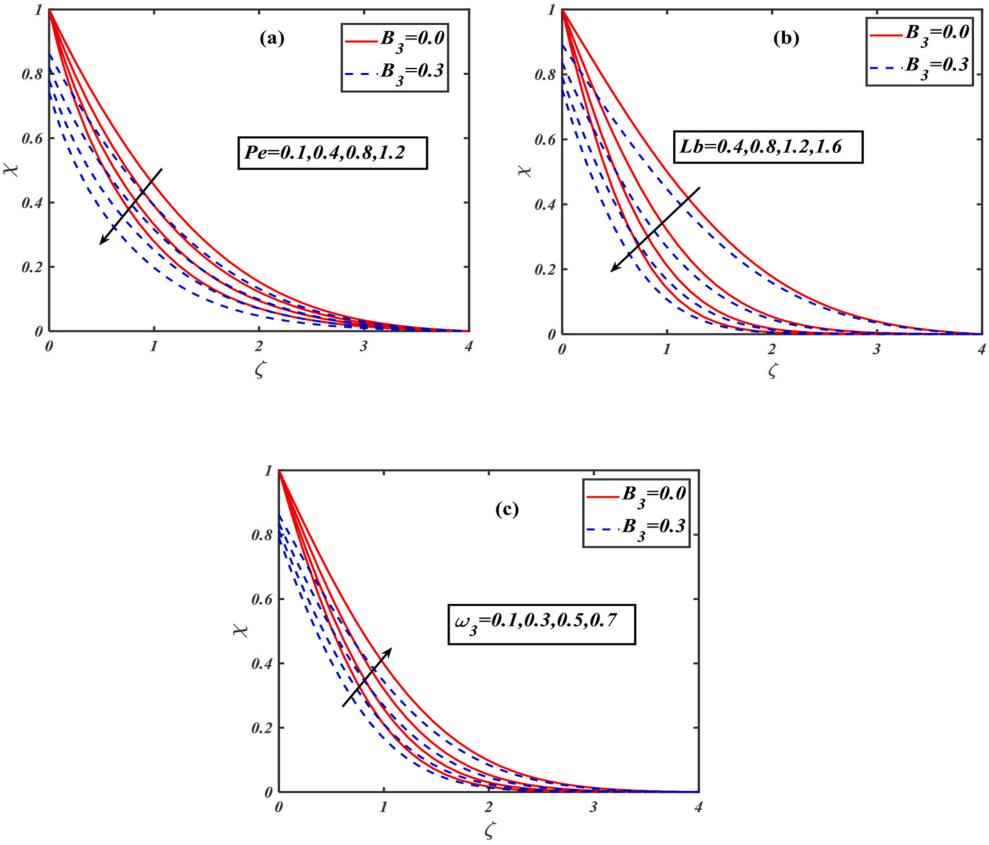

Fig. 5. Significane of Pe, Lb, ω_3 on χ.

$$\left.\begin{aligned}
&We=\sqrt{\frac{\Gamma^2\left(m+1U_0^3x^{3m-1}\right)}{2\nu}},\ Pr=\frac{\mu_0 cp}{k_\infty},\ Le=\frac{\alpha}{D_B},Ha=\frac{2\sigma B_0^2}{\rho U_0(m+1)x^{m=1}},\omega=\frac{T_w-T_\infty}{T_\infty},\\
&S=\frac{\beta^* g(1-C_\infty)(T_w-T_\infty)}{(m+1)u_e^2},\mathrm{Rb}=\frac{\left(\rho_p-\rho_f\right)(C_w-C_\infty)}{(1-C_\infty)(T_w-T_\infty)\beta^*},\mathrm{Rc}=\frac{\gamma^{**}\left(\rho_m-\rho_f\right)(N_w-N_\infty)}{(1-C_\infty)\left(T_w-\tilde{T}_\infty\right)\beta},\\
&Nb=\frac{\tau D_B(C_w-C_\infty)}{\alpha},Nt=\frac{\tau D_T(T_w-T_\infty)}{T_\infty\alpha},\gamma=\frac{2m}{m+1},\delta_0=\frac{Q}{u_e\rho c_p},\delta_1=\frac{N_\infty}{N_w-N_\infty},\\
&Pe=\frac{bW_c}{D_m},\mathrm{Lb}=\frac{\nu}{D_m},\alpha_1=\frac{L}{x}\sqrt{\mathrm{Re}_x},\ B_1=\frac{P}{x}\sqrt{\mathrm{Re}_x},\ B_2=\frac{Q_1}{x}\sqrt{\mathrm{Re}_x},B_3=\frac{R}{x}\sqrt{\mathrm{Re}_x},
\end{aligned}\right\}, \tag{18}$$

2.8. Engineering physical quantities of interest

The engineering expressions for drag force, Nusselt, Sherwood and motile numbers are calculated from following definitions:

$$\left.Cf_x=\frac{\tau_w}{\rho u_w^2/2},Nu_x=\frac{xq_w}{k(T_w-T_\infty)},Sh_x=\frac{xq_m}{D_B(C_w-C_\infty)},\mathrm{Sh}_n=\frac{xq_n}{D_m(N_w-N_\infty)}\right\}, \tag{19}$$

In which τ_w,q_w,q_m and $q_n$are defined below:

$$\begin{aligned}
&\tau_w=\mu_0\frac{\partial u}{\partial y}\left(\left(1+\left(\Lambda\frac{\partial u}{\partial y}\right)\right)^{-1}\right)\Bigg|_{y=0},q_w=-k\left(\frac{\partial T}{\partial y}\right)\Bigg|_{y=0},q_m=-D\left(\frac{\partial C}{\partial y}\right)\Bigg|_{y=0},\\
&q_n=-D_m\left(\frac{\partial N}{\partial y}\right)\Bigg|_{y=0},
\end{aligned} \tag{20}$$

In dimensionless forms one has

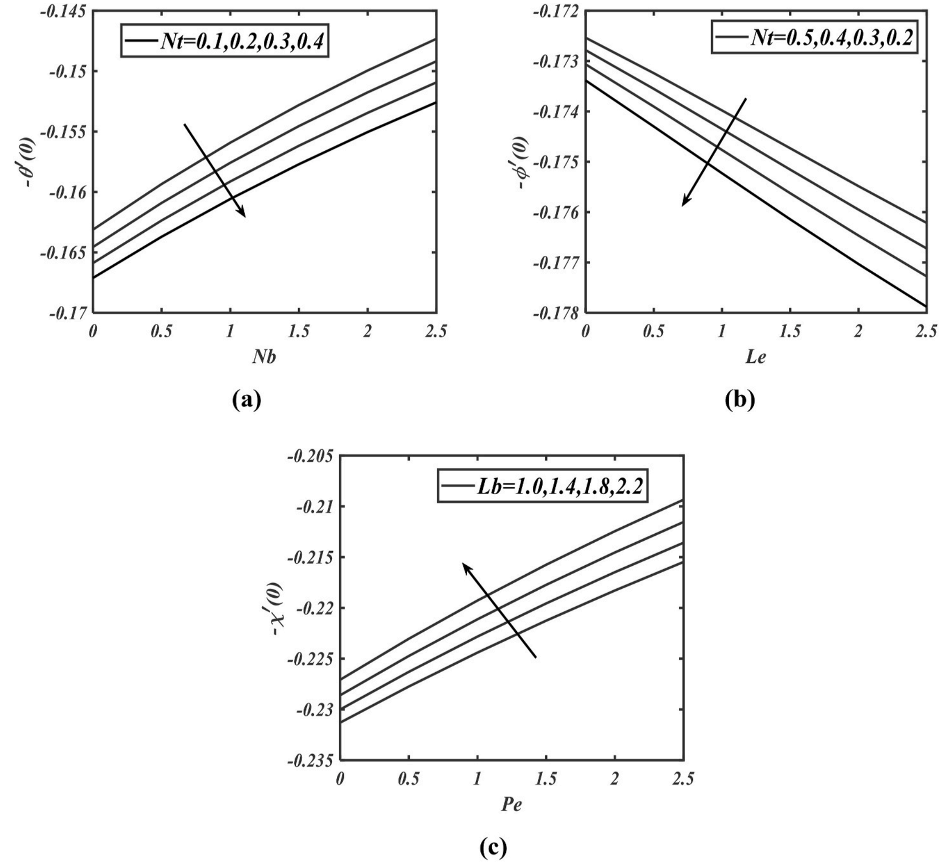

Fig. 6. Significane of *Nb*, *Nt*, *Le*, *Pe*, *Lb* on $-\theta^{'}(0)$, $-\varphi^{'}(0)$ and $-\chi^{'}(0)$.

Table 1
Comparison of numerical computation $-f''(0)$ with results of Shahzad et al. [51].

Parameters			$n=0.9$		Present values	
We	*Ha*	γ	$\alpha_1=0.0$	$\alpha_1=1.0$	$\alpha_1=0.0$	$\alpha_1=1.0$
0.0	0.3	1.0	2.536528	1.666042	2.536527	1.666040
0.1			2.400638	1.626165	2.400634	1.625863
0.4			2.092247	1.523816	2.092245	1.523618
0.8	0.5		4.043851	1.426457	4.043853	1.426458
	0.9		3.125334	1.519509	3.125343	1.519510
	1.4		2.433076	1.661463	2.433067	1.661465
0.8	0.3	1.2	2.088515	1.522247	2.088517	1.522246
		1.6	3.879954	1.651639	3.879952	1.651637
		1.8	4.684523	1.458006	4.68525	1.458004

$$\left.\begin{aligned} \mathrm{Re}_x^{1/2}Cf_x &= \frac{2}{\sqrt{2-\gamma}}f''(0)\left[\frac{1}{1+(Wef''(0))^n}\right], \\ \mathrm{Re}_x^{-1/2}Nu_x &= -\frac{2}{\sqrt{2-\gamma}}\theta^{'}(0), \\ \mathrm{Re}_x^{-1/2}Sh_x &= -\frac{2}{\sqrt{2-\gamma}}\varphi^{'}(0), \\ \mathrm{Re}_x^{-1/2}Sh_n &= -\frac{2}{\sqrt{2-\gamma}}\chi^{'}(0), \end{aligned}\right\}, \tag{21}$$

Table 2
Variations of $-f''(0)$ for Ha, n, We, S, Rb, Rc, α_1, γ.

Ha	n	We	S	Rb	Rc	α_1	γ	$-f''(0)$
0.1	0.5	1.0	0.1	0.1	0.1	0.3	0.2	
0.2	0.5	1.0	0.1	0.1	0.1	0.3	0.2	0.9548
0.6								1.0417
1.0								1.1162
0.1	0.1	1.0	0.1	0.1	0.1	0.3	0.2	0.8670
	0.4							0.9111
	0.7							0.9504
0.1	0.5	0.5	0.1	0.1	0.1	0.3	0.2	0.9361
		1.5						0.9250
		2.5						0.9111
0.1	0.5	1.0	0.2	0.1	0.1	0.3	0.2	0.9406
			0.5					0.9866
			0.8					1.0305
0.1	0.5	1.0	0.1	0.2	0.1	0.3	0.2	0.9218
				0.5				0.9126
				0.7				0.9064
0.1	0.5	1.0	0.1	0.1	0.2	0.3	0.2	0.9228
					0.5			0.9167
					0.7			0.9126
0.1	0.5	1.0	0.1	0.1	0.1	0.1	0.2	1.2606
						0.4		0.8235
						0.7		0.6294
0.1	0.5	1.0	0.1	0.1	0.1	0.3	0.1	0.8160
							0.4	0.9597
							0.7	1.0106

3. Numerical approach

The local similar solution of Eqs. (13)-(16) supported by the restricting conditions (17) is accomplished through the bvp4c technique [53]. The consequences of effective parameters that are involved in current scrutinization are exhibited through graphical and tabular data for the velocity field, temperature distribution, concentration of nanoparticles and rescaled density of motile microorganisms. Dimensionless ODEs of current flow problems are highly nonlinear in nature. The exact solution of the non-linear system of flow problems is the main challenge of research. The built-in numerical scheme known as bvp4c [54] under the commercial software MATLAB is more applicable to get the numerical solution of the current model. The bvp4c scheme is a different code that implements the Lobbato-IIIa formula. Initially higher order differential equations in velocity, temperature, volumetric concentration and motile microorganisms respectively are reduced into the first-order flow problem before starting the process. The detail of these simulations is given. Let

$$\left.\begin{array}{l} f = q_1, f' = q_2, f'' = q_3, f''' = q_3', \\ \theta = q_4, \theta' = q_5, \theta'' = q_5', \\ \varphi = q_6, \varphi' = q_7, \varphi'' = q_7', \\ \chi = q_8, \chi' = q_9, \chi'' = q_9', \end{array}\right\}, \tag{22}$$

$$q_3' = \frac{1}{\beta_1}\left[\left[-q_1q_3 - Ha^2(1-q_2) - \gamma\left(1-q_2^2\right)\right]\left[1+(Weq_3)^n\right]^2 - S\left[q_4 - Rbq_6 - Rcq_8\right]\right], \tag{23}$$

$$q_5' = \frac{1}{\beta_2}\left[-\omega_1 q_5^2 - Prq_1q_5 - Pr(Nbq_5q_7 + Ntq_5) - \delta_0 Prq_4\right], \tag{24}$$

$$q_7' = \frac{1}{\beta_3}\left[-\omega_2 q_6^2 - LePr[q_1q_7] - \frac{Nt}{Nb}q_5' + LePr\sigma(1+\omega q_4)^m \exp\left(\frac{-E}{1+\omega q_4}\right)q_6\right], \tag{25}$$

$$q_9' = \frac{1}{\beta_4}\left[-\omega q_9^2 - Lbq_1q_9 + Pe\left[q_7'(q_8+\delta_1) + q_9q_7\right]\right], \tag{26}$$

Here

$$\left.\begin{array}{l} \beta_1 = [1 + (1-n)(We_1q_3)^n], \\ \beta_2 = (1+\omega_1 q_4), \\ \beta_3 = (1+\omega_2 q_6), \\ \beta_4 = (1+\omega_3 q_9), \end{array}\right\}, \tag{27}$$

Table 3
Variations of $-\theta^{'}(0)$ for Ha, n, We, S, Rb, Rc, γ, Pr, Nb, Nt, D, B_1.

Ha	n	We	S	Rb	Rc	γ	Pr	Nb	Nt	ω_1	B_1	$-\theta^{'}(0)$
0.1	0.5	1.0	0.1	0.1	0.1	0.2	1.2	0.2	0.3	0.3	0.3	
0.2	0.5	1.0	0.1	0.1	0.1	0.2	1.2	0.2	0.3	0.3	0.3	0.7400
0.6												0.7520
1.0												0.7602
0.1	0.1	1.0	0.1	0.1	0.1	0.2	1.2	0.2	0.3	0.3	0.3	0.7302
	0.4											0.7345
	0.7											0.7390
0.1	0.5	0.5	0.1	0.1	0.1	0.2	1.2	0.2	0.3	0.3	0.3	0.7261
		1.5										0.7442
		2.5										0.7574
0.1	0.5	1.0	0.2	0.1	0.1	0.2	1.2	0.2	0.3	0.3	0.3	0.7383
			0.5									0.7451
			0.8									0.7515
0.1	0.5	1.0	0.1	0.2	0.1	0.2	1.2	0.2	0.3	0.3	0.3	0.7355
				0.5								0.7339
				0.7								0.7329
0.1	0.5	1.0	0.1	0.1	0.2	0.2	1.2	0.2	0.3	0.3	0.3	0.7356
					0.5							0.7347
					0.7							0.7341
0.1	0.5	1.0	0.1	0.1	0.1	0.1	1.2	0.2	0.3	0.3	0.3	0.7201
						0.4						0.7408
						0.7						0.7473
0.1	0.5	1.0	0.1	0.1	0.1	0.2	2.0	0.2	0.3	0.3	0.3	0.9057
							3.0					1.0416
							4.0					1.1293
0.1	0.5	1.0	0.1	0.1	0.1	0.2	1.2	0.1	0.3	0.3	0.3	0.7707
								0.4				0.6685
								0.7				0.5735
0.1	0.5	1.0	0.1	0.1	0.1	0.2	1.2	0.2	0.1	0.3	0.3	0.7878
									0.4			0.7112
									0.7			0.6418
0.1	0.5	1.0	0.1	0.1	0.1	0.2	1.2	0.2	0.2	0.1	0.3	0.7483
										0.4		0.7301
										0.7		0.7137
0.1	0.5	1.0	0.1	0.1	0.1	0.2	1.2	0.2	0.2	0.3	0.1	0.7939
											0.3	0.7077
											0.7	0.6289

with boundaries

$$\left.\begin{array}{l} q_1(0)=0,\ q_2(0)=\dfrac{\alpha_1}{\sqrt{2-\gamma}}q_3\left[\dfrac{1}{1+(Weq_3)^n}\right], \\ q_4(0)=1+\dfrac{B_1}{\sqrt{2-\chi}}q_5, q_6(0)=1+\dfrac{B_2}{\sqrt{2-\gamma}}q_7, \\ q_8(0)=1+\dfrac{B_3}{\sqrt{2-\gamma}}q_9 \end{array}\right\}, \tag{28}$$

$$q_2\rightarrow 1,\ q_4\rightarrow 0,\ q_6\rightarrow 0,\ q_8\rightarrow 0\ as\ \zeta\rightarrow\infty \tag{29}$$

4. Results and discussion

This section is reserved to discuss the significance of different parameters that appear in this article. Impacts of local Weissenberg number, Prandtl number, Lewis number, Hartmann number, bioconvection Rayleigh number, thermal conductivity parameter, microorganism conductivity parameter, wedge angle parameter, mixed convection parameter, bioconvection Lewis number, Peclet number, activation energy and Brownian motion on the velocity of the fluid, temperature profile, concentration profile and motile microorganisms profile are depicted in the graphical illustration.

Fig. 2(a–e) are captured to depicts the behavior of physical parameters namely, Hartmann numberHa, wedge angle parameterγ, mixed convection parameter S, bioconvection Rayleigh number Rc and buoyancy ratio parameter Rb against velocity field $f^{'}(\zeta)$. Fig. 2 (a) illustrates the nature of the velocity distribution $f^{'}(\zeta)$ for different values of the Hartmann numberHa. In the present sketch, solutions are analyzed for $Ha=0.1, 0.4, 0.8$ *and* 1.2. For the swelling amount of Hartmann number, the velocity profile $f^{'}(\zeta)$ is declined for both cases $\alpha_1=0.0$ and $\alpha_1=0.3$. Physically, an increment in Hartmann number produces stronger Lorentz force which cause a

Table 4
Variations of $-\varphi'(0)$ for Ha, n, We, S, Rb, Rc, γ, Pr, Nb, Nt, Le, E_a, B_2.

Ha	n	We	S	Rb	Rc	γ	Pr	Nb	Nt	Le	E_a	B_2	$-\varphi'(0)$
0.1	0.5	1.0	0.1	0.1	0.1	0.2	1.2	0.2	0.3	0.1	0.1	0.3	
0.2	0.5	1.0	0.1	0.1	0.1	0.2	1.2	0.2	0.3	0.1	0.1	0.3	0.5029
0.6													0.5082
1.0													0.5117
0.1	0.1	1.0	0.1	0.1	0.1	0.2	1.2	0.2	0.3	0.1	0.1	0.3	0.4983
	0.4												0.5004
	0.7												0.5024
0.1	0.5	0.5	0.1	0.1	0.1	0.2	1.2	0.2	0.3	0.1	0.1	0.3	0.4977
		1.5											0.5040
		2.5											0.5087
0.1	0.5	1.0	0.2	0.1	0.1	0.2	1.2	0.2	0.3	0.1	0.1	0.3	0.5023
			0.5										0.5059
			0.8										0.5093
0.1	0.5	1.0	0.1	0.2	0.1	0.2	1.2	0.2	0.3	0.1	0.1	0.3	0.5007
				0.5									0.4998
				0.7									0.4991
0.1	0.5	1.0	0.1	0.1	0.2	0.2	1.2	0.2	0.3	0.1	0.1	0.3	0.5009
					0.5								0.5004
					0.7								0.5000
0.1	0.5	1.0	0.1	0.1	0.1	0.1	1.2	0.2	0.3	0.1	0.1	0.3	0.4962
						0.4							0.5017
						0.7							0.5106
0.1	0.5	1.0	0.1	0.1	0.1	0.2	2.0	0.2	0.3	0.1	0.1	0.3	0.7151
							3.0						0.9650
							4.0						1.1934
0.1	0.5	1.0	0.1	0.1	0.1	0.2	1.2	0.1	0.3	0.1	0.1	0.3	0.0700
								0.4					0.7842
								0.7					0.9032
0.1	0.5	1.0	0.1	0.1	0.1	0.2	1.2	0.2	0.1	0.1	0.1	0.3	0.8060
									0.4				0.3754
									0.7				0.0935
0.1	0.5	1.0	0.1	0.1	0.1	0.2	1.2	0.2	0.2	0.2	0.1	0.3	0.3230
										0.4			0.2475
										0.6			0.1711
0.1	0.5	1.0	0.1	0.1	0.1	0.2	1.2	0.2	0.2	0.1	0.2	0.3	0.4966
											1.0		0.4723
											2.0		0.4590
0.1	0.5	1.0	0.1	0.1	0.1	0.2	1.2	0.2	0.2	0.1	0.1	0.1	0.5986
												0.4	0.4633
												0.7	0.3779

reduction in flow velocity of the fluid. Therefore, the velocity field reduces.

The consequences of the wedge angle parameter γ against the velocity field $f'(\zeta)$ are revealed in Fig. 2(b). The growth of the wedge angle parameter γ leads to decay in velocity field $f'(\zeta)$ for both cases $\alpha_1 = 0.0$ and $\alpha_1 = 0.3$. Fig. 2(c) accounts for the characteristics of mixed convection parameter S on the velocity field $f'(\zeta)$. The velocity field $f'(\zeta)$ increases for growing estimations of mixed convection parameter S for both cases $\alpha_1 = 0.0$ and $\alpha_1 = 0.3$. The effects of the buoyancy ratio parameter Rb on the velocity profile $f'(\zeta)$ with different values $Rb = 0.1, 0.4, 0.8$ *and* 1.2 are exhibited in Fig. 2(d). It is detected that the velocity profile $f'(\zeta)$ declines by varying the values of the buoyancy ratio parameter Rb on both conditions $\alpha_1 = 0.0$ and $\alpha_1 = 0.3$. Fig. 2(e) is captured to elucidate the features of bioconvection Rayleigh number Rc against velocity field $f'(\zeta)$ with various estimations of $Rc = 0.1, 0.4, 0.8$ *and* 1.2. The velocity profile $f'(\zeta)$ deteriorates for progressive variation of bioconvection Rayleigh number Rc.

Fig. 3(a–d) are displayed to visualize the impacts of involved parameters such as Prandtl number Pr, wedge angle parameter γ, thermophoresis parameter Nt and thermal conductivity parameter ω_1 on the temperature field $\theta(\zeta)$ for both cases $B_1 = 0.0$ and $B_1 = 0.3$. Fig. 3(a) describes the impact of the Prandtl number Pr over temperature profile $\theta(\zeta)$. The enhancing magnitude of the Prandtl number Pr diminishes the temperature distribution $\theta(\zeta)$. The sketch lines of the thermophoresis parameter Nt versus temperature distribution $\theta(\zeta)$ are delineated in Fig. 3(b). This sketch shows the enhancing trend for temperature field $\theta(\zeta)$ towards $Nt = 0.1, 0.5, 1.0$ *and* 1.5 for both situations $B_1 = 0.0$ and $B_1 = 0.3$. The features of the thermal conductivity parameter ω_1 on the temperature field $\theta(\zeta)$ are demonstrated in Fig. 3(c). From this analysis, it is revealed that temperature distribution $\theta(\zeta)$ is enhanced for both cases $B_1 = 0.0$ and $B_1 = 0.3$ by enhancing the values of the thermal conductivity parameter ω_1. Fig. 3(d) manifests the nature of the wedge angle parameter γ on temperature profile $\theta(\zeta)$ with various amount of $\gamma = 0.1, 0.3, 0.6$ *and* 0.9. The temperature distribution $\theta(\zeta)$ is knockdown by enhancing the variations of wedge angle parameter γ in both cases $B_1 = 0.0$ and $B_1 = 0.3$.

Fig. 4(a–e) demonstrate the characteristics of prominent parameters like Brownian motion parameter Nb, thermophoresis parameter Nt, activation energy E_a, Lewis number Le and thermal conductivity parameter ω_2 on the volumetric concentration of

Table 5
Variations of $-\chi'(0)$ for Ha, n, We, S, Rb, Rc, γ, Pe, Lb, B_3.

Ha	n	We	S	Rb	Rc	γ	Pe	Lb	B_3	$-\chi'(0)$
0.1	0.5	1.0	0.1	0.1	0.1	0.2	0.3	1.0	0.3	
0.2	0.5	1.0	0.1	0.1	0.1	0.2	0.3	1.0	0.3	0.8505
0.6										0.8630
1.0										0.8714
0.1	0.1	1.0	0.1	0.1	0.1	0.2	0.3	1.0	0.3	0.8403
	0.4									0.8448
	0.7									0.8495
0.1	0.5	0.5	0.1	0.1	0.1	0.2	0.3	1.0	0.3	0.8362
		1.5								0.8547
		2.5								0.8682
0.1	0.5	1.0	0.2	0.1	0.1	0.2	0.3	1.0	0.3	0.8588
			0.5							0.8559
			0.8							0.8627
0.1	0.5	1.0	0.1	0.2	0.1	0.2	0.3	1.0	0.3	0.8458
				0.5						0.8442
				0.7						0.8431
0.1	0.5	1.0	0.1	0.1	0.2	0.2	0.3	1.0	0.3	0.8460
					0.5					0.8450
					0.7					0.8424
0.1	0.5	1.0	0.1	0.1	0.1	0.1	0.3	1.0	0.3	0.8340
						0.4				0.8489
						0.7				0.8502
0.1	0.5	1.0	0.1	0.1	0.1	0.2	0.2	1.0	0.3	0.9054
							0.6			0.7070
							1.0			0.5811
0.1	0.5	1.0	0.1	0.1	0.1	0.2	0.3	1.2	0.3	0.9371
								1.6		1.0991
								2.0		1.2913
0.1	0.5	1.0	0.1	0.1	0.1	0.2	0.3	1.0	0.1	0.8470
									0.4	0.8472
									0.7	0.8495

nanoparticles $\varphi(\zeta)$ for both cases $B_2 = 0.0$ and $B_2 = 0.3$. The behavior of the Brownian motion parameter Nbon the volumetric concentration of nanoparticles $\varphi(\zeta)$ is depicted in Fig. 4(a). As expected concentration field of nanoparticles $\varphi(\zeta)$ is reducing function of the Brownian motion parameter Nb for both cases $B_2 = 0.0$ and $B_2 = 0.3$. Fig. 4(b) is the representation of concentration profile $\varphi(\zeta)$ due to thermophoresis parameter Nt at different values of$Nt = 0.1, 0.3, 0.5$ *and* 0.7. The concentration field of nano-shape particles $\varphi(\zeta)$ upsurges by growing thermophoresis parameter Nt. The physical significance of the Lewis number Le versus nanoparticle concentration $\varphi(\zeta)$ is interpreted in Fig. 4(c). Here for both cases $B_2 = 0.0$ and $B_2 = 0.3$, the concentration profile $\varphi(\zeta)$ is retarded when the Lewis number Le enhances. Fig. 4(d) is devoted to scrutinize the estimation in the concentration field $\varphi(\zeta)$ for different values of the thermal conductivity parameter ω_2. It is analyzed that the concentration field $\varphi(\zeta)$ increases for higher peaches of thermal conductivity parameter ω_2. Fig. 4(e) is engrossed to depict the impact of activation energy E_a on the volumetric concentration field of nanoparticles $\varphi(\zeta)$ for both situations $B_2 = 0.0$ and $B_2 = 0.3$. It can be perceived that volumetric concentration $\varphi(\zeta)$ is enhanced by an increment in the activation energy E_a.

Fig. 5(a–c) are elucidated to interpret the significance of bioconvection Lewis number Lb, Peclet number Pe and microorganism conductivity parameter ω_3 on the motile microorganisms field $\chi(\zeta)$ for both cases $B_3 = 0.0$ and $B_3 = 0.3$. The curves of motile microorganism's field $\chi(\zeta)$ versus Peclet number Pe are elaborated in Fig. 5(a). It is found that the microorganisms field $\chi(\zeta)$ declines by an increment in the variation of Peclet number Pe for $B_3 = 0.0$ and $B_3 = 0.3$. Fig. 5(b) prevail the interesting scenario about the bioconvection Lewis number Lb on motile microorganism field $\chi(\zeta)$ for $B_3 = 0.0$ and $B_3 = 0.3$. It is noticed that the rescaled density of motile microorganisms $\chi(\zeta)$ reduces by enlarging the bioconvection Lewis number Lb. Fig. 5(c) is examined the effect of the microorganism conductivity parameter ω_3 on the swimming microorganisms profile $\chi(\zeta)$. It is concluded that the motility of fluid $\chi(\zeta)$ decreases at higher peaches of microorganism conductivity parameter ω_3 for both cases $B_3 = 0.0$ and $B_3 = 0.3$.

Fig. 6(a–c) show the effects of Nb, Nt, Le, Pe, Lb on $-\theta'(0)$, $-\varphi'(0)$ and $-\chi'(0)$ respectively. Here $-\theta'(0)$ and $-\varphi'(0)$ are enhanced for larger values of thermophoresis parameter. Furthermore, the $-\chi'(0)$ is an increasing function of Lb.

In Table 1, to attained the numerical solution of the skin friction coefficient for a chosen variation of Weissenberg number We, Hartmann number Ha and wedge angle parameter γ is compared with those studied by Shahzad et al. [51] and found to be in good agreement.

Table 2 is drawn to observe the behavior of involving parameters such as Ha, n, We, S, Rb, Rc, α_1, γ on skin friction coefficient. It is noticed that the skin friction coefficient enhances for the variation of Ha, Rb andγ.

The features of Nusselt number against prominent parameters are presented in Table 3. The Nusselt number rises for a different variation of ω_1, S while decreases for Pr.

Table 4 is constructed to examine the behavior of Ha, n, We, S, Rb, Rc, γ, Pr, Nb, Nt, D and B_1 versus Sherwood number. With growing amount of

Ha, the Sherwood number reduces.

Table 5 explicates the significance of rescaled density number of motile microorganisms versus $Ha, n, We, S, \mathrm{Rb}, Rc, \gamma, Pe, Lb, B_3$. The rescaled density number of motile microorganisms is reduced for higher variations of Pe, Lb.

5. Conclusions

This article discusses the heat and mass transfer features in non-Newtonian (cross fluid) nano-material flow with multiple slip conditions. The salient features of motile microorganism, nonlinear heat source/sink and activation energy are accounted. The key points of current article are.

- Velocity profile exaggerates for higher values of mixed convection parameter while opposite behavior is observed for buoyancy ratio parameter and bioconvection Lewis number.
- The temperature distribution is a reducing function of the Prandtl number [55].
- The temperature field is enhanced for thermophoresis parameter and thermal conductivity parameter.
- The volumetric concentration of nanoparticles increases for growing thermal conductivity parameter.
- The density of motile microorganisms depicts diminishing trend for bioconvection Lewis number and Peclet number [56–65].
- The current mathematical flow model is more useful in the field of nanotechnology, electrical and mechanical engineering, biotechnology, biofuel, microbiology etc.
- In future, one can extend this work by considering magnetic dipole, convective boundary conditions, homogeneous-heterogeneous reactions, nonlinear thermal radiation etc.

Declaration of competing interest

The authors declare that they have no known competing financial interests or personal relationships that could have appeared to influence the work reported in this paper.

Acknowledgement

The Deanship of Scientific Research (DSR) at King Abdulaziz University, Jeddah, Saudi Arabia funded this project, under grant no. FP-27-42.

References

[1] S.U.S. Choi, J.A. Eastman, Enhancing Thermal Conductivity of Fluids with Nanoparticles, Argonne National Lab., IL (United States), 1995.
[2] J. Buongiorno, Convective transport in nanofluids, J. Heat Tran. 128 (2006) 240–250.
[3] C.S.K. Raju, M.J. Babu, N. Sandeep, P.M. Krishna, Influence of non-uniform heat source/sink on MHD nanofluid flow over a moving vertical plate in porous medium, Int. J. Sci. Eng. Res. 6 (2015) 31–42.
[4] D.D. Ganji, M. Sheikholeslami, Applications of Nanofluid for Heat Transfer Enhancement, Elsevier, 2017.
[5] M. Sheikholeslami, M.M. Bhatti, Forced convection of nanofluid in presence of constant magnetic field considering shape effects of nanoparticles, Int. J. Heat Mass Tran. 111 (2017) 1039–1049.
[6] K.L. Hsiao, To promote radiation electrical MHD activation energy thermal extrusion manufacturing system efficiency by using Carreau-nanofluid with parameters control method, Energy 130 (2017) 486–499.
[7] M. Turkyilmazoglu, Buongiorno model in a nanofluid filled asymmetric channel fulfilling zero net particle flux at the walls, Int. J. Heat Mass Tran. 126 (2018) 974–979.
[8] S.U. Khan, S.A. Shehzad, Brownian movement and thermophoretic aspects in third-grade nanofluid over oscillatory moving sheet, Phys. Scripta 94 (2019), 095202.
[9] H. Waqas, S.A. Shehzad, S.U. Khan, M. Imran, Novel numerical computations on flow of nanoparticles in porous rotating disk with multiple slip effects and microorganisms, J. Nanofluids. 8 (2019) 1423–1432.
[10] M. Hassan, M. Marin, A. Alsharif, R. Ellahi, Convective heat transfer flow of nanofluid in a porous medium over wavy surface, Phys. Lett. A. 382 (2018) 2749–2753.
[11] M. Sheikholeslami, H.B. Rokni, Numerical simulation for impact of Coulomb force on nanofluid heat transfer in a porous enclosure in presence of thermal radiation, Int. J. Heat Mass Tran. 118 (2018) 823–831.
[12] T. Hayat, S. Nadeem, A.U. Khan, Rotating flow of Ag-CuO/H2O hybrid nanofluid with radiation and partial slip boundary effects, Eur. Phys. J. E. 41 (2018) 75.
[13] R.S. Saif, T. Muhammad, H. Sadia, R. Ellahi, Hydromagnetic flow of Jeffrey nanofluid due to a curved stretching surface, Phys. A Stat. Mech. its Appl. 551 (2020) 124060.
[14] S.M.R.S. Naqvi, H.M. Kim, T. Muhammad, F. Mallawi, M.Z. Ullah, Numerical study for slip flow of Reiner-Rivlin nanofluid due to a rotating disk, Int. Commun. Heat Mass Tran. 116 (2020) 104643.
[15] M. Asma, W.A.M. Othman, T. Muhammad, F. Mallawi, B.R. Wong, Numerical study for magnetohydrodynamic flow of nanofluid due to a rotating disk with binary chemical reaction and Arrhenius activation energy, Symmetry 11 (2019) 1282.
[16] M.R. Eid, K.L. Mahny, A. Dar, T. Muhammad, Numerical study for Carreau nanofluid flow over a convectively heated nonlinear stretching surface with chemically reactive species, Phys. A Stat. Mech. its Appl. 540 (2020) 123063.
[17] T. Hayat, A. Aziz, T. Muhammad, A. Alsaedi, Numerical simulation for three-dimensional flow of Carreau nanofluid over a nonlinear stretching surface with convective heat and mass conditions, J. Brazilian Soc. Mech. Sci. Eng. 41 (2019) 55.
[18] M. Sheikholeslami, New computational approach for exergy and entropy analysis of nanofluid under the impact of Lorentz force through a porous media, Comput. Methods Appl. Mech. Eng. 344 (2019) 319–333.
[19] K.G. Kumar, G.K. Ramesh, S.A. Shehzad, F.M. Abbasi, Three-dimensional (3D) rotating flow of selenium nanoparticles past an exponentially stretchable surface due to solar energy radiation, J. Nanofluids. 8 (2019) 1034–1040.
[20] T. Hayat, M. Waqas, A. Alsaedi, G. Bashir, F. Alzahrani, Magnetohydrodynamic (MHD) stretched flow of tangent hyperbolic nanoliquid with variable thickness, J. Mol. Liq. 229 (2017) 178–184.

[21] K.G. Kumar, B.J. Gireesha, R.S.R. Gorla, Flow and heat transfer of dusty hyperbolic tangent fluid over a stretching sheet in the presence of thermal radiation and magnetic field, Int. J. Mech. Mater. Eng. 13 (2018) 2.
[22] T. Muhammad, A. Alsaedi, T. Hayat, S.A. Shehzad, A revised model for Darcy-Forchheimer three-dimensional flow of nanofluid subject to convective boundary condition, Results Phys 7 (2017) 2791–2797.
[23] O.D. Makinde, B. Mahanthesh, B.J. Gireesha, N.S. Shashikumar, R.L. Monaledi, M.S. Tshehla, MHD nanofluid flow past a rotating disk with thermal radiation in the presence of aluminum and titanium alloy nanoparticles, Defect Diffusion Forum 384 (2018) 69–79.
[24] B. Mahanthesh, G. Lorenzini, F.M. Oudina, I.L. Animasaun, Significance of exponential space-and thermal-dependent heat source effects on nanofluid flow due to radially elongated disk with Coriolis and Lorentz forces, J. Therm. Anal. Calorim. 141 (2020) 37–44.
[25] S.A. Shehzad, B. Mahanthesh, B.J. Gireesha, N.S. Shashikumar, M. Madhu, Brinkman-Forchheimer slip flow subject to exponential space and thermal-dependent heat source in a microchannel utilizing SWCNT and MWCNT nanoliquids, Heat Transf.-Asian Res. 48 (2019) 1688–1708.
[26] C.S.K. Raju, M.M. Hoque, P. Priyadharshini, B. Mahanthesh, B.J. Gireesha, Cross diffusion effects on magnetohydrodynamic slip flow of Carreau liquid over a slendering sheet with non-uniform heat source/sink, J. Brazilian Soc. Mech. Sci. Eng. 40 (2018) 222.
[27] F. Sultan, S. Mustafa, W.A. Khan, M. Shahzad, M. Ali, W. Adnan, S. Rehman, A numerical treatment on rheology of mixed convective Carreau nanofluid with variable viscosity and thermal conductivity, Appl. Nanosci. (2020), https://doi.org/10.1007/s13204-020-01294-1.
[28] B. Mahanthesh, N.S. Shashikumar, B.J. Gireesha, I.L. Animasaun, Effectiveness of Hall current and exponential heat source on unsteady heat transport of dusty TiO2-EO nanoliquid with nonlinear radiative heat, J. Comput. Des. Eng. 6 (2019) 551–561.
[29] B. Mahanthesh, B.J. Gireesha, I.L. Animasaun, T. Muhammad, N.S. Shashikumar, MHD flow of SWCNT and MWCNT nanoliquids past a rotating stretchable disk with thermal and exponential space dependent heat source, Phys. Scripta 94 (2019), 085214.
[30] K.A. Maleque, Effects of exothermic/endothermic chemical reactions with Arrhenius activation energy on MHD free convection and mass transfer flow in presence of thermal radiation, J. Thermodyn. 2013 (2013) 692516.
[31] F.G. Awad, S. Motsa, M. Khumalo, Heat and mass transfer in unsteady rotating fluid flow with binary chemical reaction and activation energy, PloS One 9 (2014), e107622.
[32] M.I. Khan, T. Hayat, M.I. Khan, A. Alsaedi, Activation energy impact in nonlinear radiative stagnation point flow of Cross nanofluid, Int. Commun. Heat Mass Tran. 91 (2018) 216–224.
[33] Z. Shafique, M. Mustafa, A. Mushtaq, Boundary layer flow of Maxwell fluid in rotating frame with binary chemical reaction and activation energy, Results Phys 6 (2016) 627–633.
[34] A.V. Kuznetsov, The onset of nanofluid bioconvection in a suspension containing both nanoparticles and gyrotactic microorganisms, Int. Commun. Heat Mass Tran. 37 (2010) 1421–1425.
[35] A.V. Kuznetsov, A.A. Avramenko, Effect of small particles on this stability of bioconvection in a suspension of gyrotactic microorganisms in a layer of finite depth, Int. Commun. Heat Mass Tran. 31 (2004) 1–10.
[36] M. Khan, M. Irfan, W.A. Khan, Impact of nonlinear thermal radiation and gyrotactic microorganisms on the Magneto-Burgers nanofluid, Int. J. Mech. Sci. 130 (2017) 375–382.
[37] N. Begum, S. Siddiqa, M.A. Hossain, Nanofluid bioconvection with variable thermophysical properties, J. Mol. Liq. 231 (2017) 325–332.
[38] M. Waqas, T. Hayat, S.A. Shehzad, A. Alsaedi, Transport of magnetohydrodynamic nanomaterial in a stratified medium considering gyrotactic microorganisms, Phys. B Condens. Matter 529 (2018) 33–40.
[39] F.T. Zohra, M.J. Uddin, A.I.M. Ismail, O.A. Bég, A. Kadir, Anisotropic slip magneto-bioconvection flow from a rotating cone to a nanofluid with Stefan blowing effects, Chin. J. Phys. 56 (2018) 432–448.
[40] M.J. Uddin, Y. Alginahi, O.A. Bég, M.N. Kabir, Numerical solutions for gyrotactic bioconvection in nanofluid-saturated porous media with Stefan blowing and multiple slip effects, Comput. Math. Appl. 72 (2016) 2562–2581.
[41] R. Naz, M. Noor, T. Hayat, M. Javed, A. Alsaedi, Dynamism of magnetohydrodynamic cross nanofluid with particulars of entropy generation and gyrotactic motile microorganisms, Int. Commun. Heat Mass Tran. 110 (2020) 104431.
[42] K. Mohamed, T. Ismail, N. Nourreddine, S.M. Rafik, Analytical study of nano-bioconvective flow in a horizontal channel using adomian decomposition method, J. Comput. Appl. Res. Mech. Eng. 9 (2020) 245–258.
[43] M.S. Ansari, O. Otegbeye, M. Trivedi, S.P. Goqo, Magnetohydrodynamic bioconvective Casson nanofluid flow: a numerical simulation by paired quasilinearisation, J. Appl. Comp. Mech. (2020), https://doi.org/10.22055/jacm.2020.31205.1839.
[44] H. Waqas, S.U. Khan, M. Hassan, M.M. Bhatti, M. Imran, Analysis on the bioconvection flow of modified second-grade nanofluid containing gyrotactic microorganisms and nanoparticles, J. Mol. Liq. 291 (2019) 111231.
[45] Y. Wang, H. Waqas, M. Tahir, M. Imran, C.Y. Jung, Effective Prandtl aspects on bio-convective thermally developed magnetized tangent hyperbolic nanoliquid with gyrotactic microorganisms and second order velocity slip, IEEE Access 7 (2019) 130008–130023.
[46] S.U. Khan, H. Waqas, M.M. Bhatti, M. Imran, Bioconvection in the rheology of magnetized couple stress nanofluid featuring activation energy and Wu's slip, J. Non-Equilibrium Thermodyn. 45 (2019) 81–95.
[47] M.K. Nayak, J. Prakash, D. Tripathi, V.S. Pandey, S. Shaw, O.D. Makinde, 3D Bioconvective multiple slip flow of chemically reactive Casson nanofluid with gyrotactic micro-organisms, Heat Transf. 49 (2020) 135–153.
[48] C.S. Balla, R. Alluguvelli, K. Naikoti, O.D. Makinde, Effect of chemical reaction on bioconvective flow in oxytactic microorganisms suspended porous cavity, J. Appl. Comput. Mech. 6 (2020) 653–664.
[49] M.I. Khan, F. Haq, S.A. Khan, T. Hayat, M.I. Khan, Development of thixotropic nanomaterial in fluid flow with gyrotactic microorganisms, activation energy, mixed convection, Comput. Methods Progr. Biomed. 187 (2020) 105186.
[50] T. Muhammad, S.Z. Alamri, H. Waqas, D. Habib, R. Ellahi, Bioconvection flow of magnetized Carreau nanofluid under the influence of slip over a wedge with motile microorganisms, J. Therm. Anal. Calorim. (2020), https://doi.org/10.1007/s10973-020-09580-4.
[51] M. Shahzad, M. Ali, F. Sultan, W.A. Khan, Z. Hussain, Computational investigation of magneto-cross fluid flow with multiple slip along wedge and chemically reactive species, Results Phys 16 (2020) 102972.
[52] M.T. Sk, K. Das, P.K. Kundu, Multiple slip effects on bioconvection of nanofluid flow containing gyrotactic microorganisms and nanoparticles, J. Mol. Liq. 220 (2016) 518–526.
[53] T.Y. Na, Computational Methods in Engineering Boundary Value Problems first ed., vol. 145, Academic Press, 1979.
[54] L. Shampine, J. Kierzenka, M. Reichelt, Solving boundary value problems for ordinary differential equations in MATLAB with bvp4c, Tutor. Notes. 75275 (2000) 1–27.
[55] M. Asma, W.A.M. Othman, T. Muhammad, Numerical study for Darcy–Forchheimer flow of nanofluid due to a rotating disk with binary chemical reaction and Arrhenius activation energy, Mathematics 7 (2019) 921.
[56] M.A. Rahman, M.J. Uddin, O.A. Beg, A. Kadir, Influence of variable viscosity and thermal conductivity, hydrodynamic, and thermal slips on magnetohydrodynamic micropolar flow: a numerical study, Heat Tran. Asian Res. 8 (2019) 3928–3944.
[57] F.T. Zohra, M.J. Uddin, Al Ismail, Magnetohydrodynamic bio-convective Naiver slip flow of micropolar fluid in stretchable horizontal channel, Heat Tran. Asian Res. 48 (2019) 3636–3656.
[58] F.T. Zohra, M.J. Uddin, M.F. Basir, Al Ismail, Magnetohydrodynamic bio-nano-convective slip flow with Stefan blowing effects over a rotating disc, Proc. Inst. Mech. Eng. Part N: J. Nanomater. Nanoeng. Nanosyst. 234 (2020) 83–97.
[59] O.A. Beg, M.J. Uddin, T.A. Beg, A. Kadir, M.D. Shamshuddin, M. Babaie, Numerical study of self-similar natural convection mass transfer from a rotating cone in anisotropic porous media with Stefan blowing and Navier Slip, Indian J. Phys. (2019) 1–15.
[60] W.A. Khan, M.J. Uddin, A.M. Ismail, Hydrodynamic and thermal slip effect on Double-diffusive free convective boundary layer flow of nanofluid past a flat vertical plate in the moving free stream, PloS One 8 (2013), e54024.

[61] M.J. Uddin, M.N. Kabir, O.A. Beg, Y. Alginahi, Chebyshev collocation computation of magneto-bioconvection nanofluid flow over a wedge with multiple slips and magnetic induction, Proc. Inst. Mech. Eng. Part N: J. Nanomater. Nanoeng. Nanosyst. 23 (2018) 109–122.
[62] A.A. Mutlag, M.J. Uddin, A.I. Ismail, Scalling transformation for free convection flow of a micropolar fluid along a moving vertical plate in a porous medium with velocity and thermal slip boundary conditions, Sains Malays. 43 (2014) 1249–1257.
[63] M.J. Uddin, M.N. Kabir, y Alginahi, O.A. Beg, Numerical solution of bio-nano-convection transport from a horizontal Plate with blowing and multiple slip effects, Proc. IME C J. Mech. Eng. Sci. 233 (2019) 6910–6927.
[64] Mustafa Turkyilmazoglu, Slip flow and heat transfer over a specific wedge: an exactly solvable Falkner–Skan equation, J. Eng. Math. 92 (2015) 73–81.
[65] Mustafa Turkyilmazoglu, Single phase nanofluids in fluid mechanics and their hydrodynamic linear stability analysis, Comput. Methods Progr. Biomed. 187 (2020) 105171.
[66] Mair Khan, T. Salahuddin, Muhammad Malik Yousaf, Farzana Khan, Arif Hussain, Variable diffusion and conductivity change in 3D rotating Williamson fluid flow along with magnetic field and activation energy, Int. J. Numer. Methods Heat Fluid Flow 30 (2019) 2467–2484.